Type of Contribution:
Editorial
Research Paper
Review Paper
Case Study

ENERGY: JURNAL ILMIAH ILMU-ILMU TEKNIK
Vol. 16, No. 2 (2026) pp 501-518
DOI: 10.51747/energy.v16i2.p501-518

E-ISSN: 2962-2565

This article contributes to:

Evaluation of Nano-Scale ZnO Coatings Prepared via the Sol–Gel Method on Cast Iron Piston Rings: Tribological Performance

Fabrobi Ridha[1]*, Nurul Hidayana [1], Haidzar Nurdiansyah[2], Zaid Sulaiman[1]

[1] Mechanical Engineering Department, Nusa Putra University, Sukabumi Regency, West Java, 43152, **Indonesia**

[2] Mechanical Design Engineering Deparment, Jember University, Jember Regency, East Java, 68121, **Indonesia**

* fabrobi.fazlur@nusaputra.ac.id

Abstract

This study evaluated the structural, thermal, and tribological performance of nano-scale ZnO coatings synthesized via a sol–gel method and deposited on FC-25 grey cast iron substrates using dip-coating followed by annealing at 400 °C. Three precursor molarities (0.1 M, 0.2 M, and 0.4 M) and two dipping cycles (1× and 2× dip) were investigated. Structural characterization confirmed the formation of crystalline hexagonal wurtzite ZnO after annealing. Thermogravimetric analysis indicated a 4.48% mass loss in non-furnaced samples due to organic precursor decomposition, whereas annealed samples exhibited a stable relative mass change (+4.68%). Scanning electron microscopy revealed post-annealing microcracks resulting from volumetric shrinkage and thermal expansion mismatch. Tribological testing under ASTM G99 conditions demonstrated that the coated specimens did not outperform the untreated cast iron substrate (friction force: 0.89±0.22" N" ; CoF: 0.18±0.05; wear depth: 6.6±2.1 μ"m"). Among the coated conditions, performance was strongly governed by process parameters: double-dipping at low molarity (2× Dip, 0.1 M) produced the highest wear and friction (friction force: 4.91±1.55" N" ; CoF: 1.00±0.32; wear depth: 131.4±69.3 μ"m"), whereas increasing precursor molarity (2× Dip, 0.4 M) substantially mitigated wear degradation (friction force: 1.63±0.57" N" ; CoF: 0.33±0.10; wear depth: 41.5±14.8 μ"m"). Two-way ANOVA confirmed that precursor molarity exerts a primary statistically significant effect ($p<0.05$) alongside a significant interaction with dipping cycle ($p<0.05$). These results demonstrate that

Article Info
Submitted: 2026-08-24
Revised: 2026-09-09
Accepted: 2026-09-25
Published: 2026-09-27

This work is licensed under a Creative Commons Attribution-NonCommercial 4.0 International License

Publisher
Universitas Panca Marga

coating structural integrity and stress management play a more critical role than bulk crystallinity in dictating tribological performance.

Keywords: ZnO coating, grey cast iron, piston ring, sol–gel method, dip-coating, tribological performance, wear, pin-on-disk.

1. Introduction

The piston ring is a key component of internal combustion engines, functioning to maintain the seal between piston and cylinder wall, regulate oil distribution, and prevent gas leakage during engine operation. Continuous sliding contact between the ring and cylinder wall leads to friction and wear, which can reduce engine efficiency, increase fuel consumption, and elevate emissions.

To address frictional losses and wear, various coating strategies have been implemented. Conventional coatings such as hard chrome plating and diamond-like carbon (DLC) have demonstrated excellent tribological properties [1], [2]. However, these established methods often involve high production costs, require advanced equipment, and raise environmental concerns, particularly from toxic chromium waste [3]. As a result, ongoing research seeks alternative coating materials that are cost-effective, environmentally friendly, and suitable for industrial-scale production [4], [5], [6], [7].

Zinc oxide (ZnO) is a semiconductor material with favorable thermal stability, abrasion resistance, and low environmental impact [8]. In nanostructured form, ZnO has the potential to enhance surface hardness and wear resistance, making it an attractive candidate for tribological coatings [9], [10]. Previous studies have reported promising effects of nano-ZnO coatings synthesized by sol-gel methods, but direct application to piston rings—particularly through accessible and economical dip-coating processes—remains relatively unexplored [11], [12].

This research investigates the preparation and tribological evaluation of sol-gel synthesized nano-ZnO coatings applied to cast iron piston rings via dip-coating and subsequent thermal treatment. The aim is to assess the coating's morphology and tribological behavior, providing a critical performance on the effectiveness and practical potential of nano-ZnO coatings for engine components. The findings contribute valuable data for future optimization strategies and the broader exploration of sustainable tribological materials in automotive applications.

2. Materials and Methods

Grey cast iron (FC-25), commonly used in piston ring applications due to its favorable mechanical and tribological properties, was selected as the substrate material [13], [14]. Disc specimens were prepared according to ASTM G99 standards with a diameter of 58 mm and a thickness of 8 mm [15]. Prior to coating, the substrate

surfaces were progressively ground using silicon carbide (SiC) abrasive papers with grit sizes ranging from 80 to 2000 to obtain a uniform surface finish. The samples were then dried in an oven at 160 °C to eliminate residual moisture.

The ZnO sol–gel precursor solution was synthesized using zinc acetate dihydrate as the zinc source and ethanol as the solvent. Monoethanolamine (MEA) was added as a stabilizing agent at a molar ratio of Zn^{2+} to MEA of 1:1 to promote solution stability and controlled hydrolysis. The mixture was magnetically stirred at 50–60 °C for 1 hour until a clear and homogeneous sol was obtained. Subsequently, the solution was aged at room temperature for 24 hours to allow sufficient hydrolysis and condensation reactions. Three precursor concentrations were prepared, namely 0.1 M, 0.2 M, and 0.4 M, each in a total volume of 200 mL [16].

Coating deposition was carried out using a dip-coating technique. Each substrate was vertically immersed into the aged sol at a controlled rate of approximately 2 mm/s and maintained in the solution for 10 seconds before being withdrawn at a constant speed. After withdrawal, the samples were air-dried for 10 minutes and subsequently oven-dried at 100 °C for 10 minutes to facilitate solvent evaporation. An additional air-drying period of 10–15 minutes was applied before subsequent dipping when required. Two coating conditions were investigated: single-layer deposition (1× dip) and double-layer deposition (2× dip). After completion of the final dipping number, the coated samples were dried at 100 °C for 60 minutes to ensure adequate removal of residual solvents.

Thermal treatment was performed to convert the gel layer into crystalline ZnO and to eliminate organic residues from the precursor. The coated samples were placed in a furnace and heated gradually to 400 °C with incremental holding at each 100 °C interval to minimize thermal shock. A final dwell time of 30 minutes at 400 °C was applied to promote crystallization and densification of the ZnO layer [17]. After completion of the heating cycle, the furnace was switched off and allowed to cool naturally to below 100 °C before unloading the samples. Both non-annealed (as-dried) and annealed (annealed) samples were evaluated to investigate the influence of thermal treatment on structural and tribological properties.

Thermogravimetric analysis (TGA) was conducted to examine the thermal decomposition behavior and mass loss characteristics of the sol–gel-derived coatings [16]. Both non-annealed and annealed samples were analyzed to identify solvent evaporation stages, organic precursor decomposition, and the thermal stability of the ZnO phase. The measurements were performed under controlled heating conditions from room temperature to elevated temperatures, allowing assessment of the effectiveness of the 400 °C annealing process in removing residual organic components and stabilizing the oxide structure.

Phase identification and crystallinity analysis were carried out using X-ray diffraction (XRD). Coated samples prepared with precursor concentrations of 0.1 M, 0.2 M, and 0.4 M were examined over an appropriate 2θ range to detect characteristic diffraction peaks corresponding to crystalline ZnO. The obtained diffraction patterns were compared with standard reference data to confirm phase formation and to evaluate the influence of precursor molarity on crystallinity and structural ordering.

Surface morphology and coating integrity were analyzed using Scanning Electron Microscopy (SEM). Observations were performed at various magnifications to assess surface uniformity, crack formation, and coating thickness distribution. Energy Dispersive Spectroscopy (EDS) was employed to determine elemental composition and to confirm the presence and distribution of Zn and O within the coating layer.

Tribological performance was evaluated using a pin-on-disk tribometer in accordance with ASTM G99 standards under dry sliding conditions at ambient temperature (25±2" °C") and relative humidity (50±5%). A high-hardness alumina (〖"Al" 〗_2 "O" _3) spherical pin with a diameter of 6" mm" was used as the counterface material. Tests were conducted under a constant normal load of 2" N" and a rotational speed of 50" RPM" for a total duration of 10" min" (600" s"). The wear track radius was fixed at 10" mm" , yielding a linear sliding velocity of approximately 0.052" m/s" and a total sliding distance of 31.4" m" . Prior to testing, all cast iron substrates were ground and polished to a baseline surface roughness (R_a) of approximately 0.1" " μ"m" and thoroughly cleaned with ethanol in an ultrasonic bath. Friction force, coefficient of friction (CoF), and wear depth were recorded continuously during testing. All tribological tests were performed in triplicate (n=3) for each sample condition to ensure statistical reproducibility.

Statistical analysis was performed using a two-way Analysis of Variance (ANOVA) to evaluate the effects of precursor molarity and dipping number, as well as their interaction, on friction force, coefficient of friction, and wear depth. Statistical significance was determined at a confidence level of 95% ($p < 0.05$), enabling quantitative assessment of the influence of processing parameters on tribological performance.

3.Results and Discussion

This section presents the structural, thermal, morphological, and tribological characterization of ZnO sol–gel coatings deposited on FC-25 cast iron substrates, together with statistical evaluation of processing parameters. The results are discussed in a systematic manner to establish the relationship between precursor molarity, coating thickness, thermal conversion behavior, and tribological

performance. By integrating macroscopic surface observations, X-ray diffraction (XRD), thermogravimetric analysis (TGA), scanning electron microscopy (SEM), and two-way ANOVA, a comprehensive understanding of the mechanisms governing coating integrity and wear resistance is developed. Particular emphasis is placed on the interplay between crystallinity, shrinkage-induced stress, interfacial adhesion, and their combined influence on coating durability.

Figure 1 presents the as-deposited ZnO sol–gel coatings prior to furnace treatment. The coatings appear macroscopically uniform and continuous across the substrate surface, indicating successful deposition and spreading of the precursor solution. No visible macroscopic cracking is observed at this stage, suggesting that the gel films remain structurally intact before thermal conversion.

Figure 1. Samples coated with nano-ZnO using dip-coating before annealing

Slight variations in surface reflectivity are observed among samples, which may be attributed to differences in precursor molarity and coating thickness. In particular, localized surface contrast variations suggest non-uniform solvent evaporation or minor wetting differences during dip-coating. These variations become important when considering subsequent densification behavior during annealing.

3.1 Tribological Findings

The table of tribological data (**Table 1**) shows that ZnO-coated samples present higher friction force, coefficient of friction (CoF), and wear depth compared to the untreated control sample. For instance, the untreated control exhibits the lowest mean friction force (−0.89±0.22N), CoF (−0.18±0.05), and minimal wear depth (−6.6±763.9 μm). In contrast, coated samples—especially those prepared with higher dipping numbers and lower molarity (e.g., 2× Dip, 0.1 M)—demonstrate an increase in friction force (−4.91±1.55 N), CoF (−1.00±0.32), and wear depth (−131.4±69.3 μm). The tendency for increased wear and friction in coated samples suggests that the

ZnO sol-gel layer, under the tested conditions, did not impart the expected improvements in tribological behavior [18].

Table 1. Tribological Test Result of nano-ZnO Coated Cast Iron

No	Dip Coating & Concentration	Friction Force (N) Mean ± SD	Coefficient of Friction (CoF) Mean ± SD	Wear Depth (μm) Mean ± SD
1	1x Dip, 0.1 M	3.38 ± 1.52	0.68 ± 0.30	97.2 ± 55.1
2	1x Dip, 0.2 M	1.66 ± 0.42	0.33 ± 0.08	23.1 ± 21.8
3	1x Dip, 0.4 M	2.32 ± 0.76	0.46 ± 0.15	31.2 ± 28.2
4	2x Dip, 0.1 M	4.91 ± 1.55	1.00 ± 0.32	131.4 ± 69.3
5	2x Dip, 0.2 M	3.25 ± 0.90	0.66 ± 0.17	93.3 ± 21.8
6	2x Dip, 0.4 M	1.63 ± 0.57	0.33 ± 0.10	41.5 ± 14.8
7	Untreated Control (No Coating)	0.89 ± 0.22	0.18 ± 0.05	6.6 ± 2.1*

*Note: An electronic measurement signal artifact (X>50,000 μ"m" at t=405" s") was removed prior to calculating the final wear depth mean and standard deviation.

Interestingly, samples with higher molarity ZnO precursor and increased dipping numbers (e.g., 2× Dip, 0.4 M) show somewhat reduced wear depth (−41.5±14.8 μm) and friction force (−1.63±0.57 N) compared to samples with lower molarity or dipping number, though performance is still inferior to the untreated control. This pattern indicates that both sol-gel molarity and dipping numbers influence layer morphology and, ultimately, tribological results—a trend quantitatively supported by the ANOVA findings.

3.2 SEM Observations

The surface morphology of the ZnO coating was observed using Scanning Electron Microscopy (SEM) at several magnifications, as shown in **Figure 2**. All samples exhibited visible cracks distributed throughout the coating surface, although the overall layer still appeared to cover the substrate uniformly. The presence of cracks indicates that while the sol-gel synthesis and coating processes were successful in depositing ZnO films, certain process parameters need optimization to improve coating integrity. The absence of visible cracking in the pre-annealed condition indicates that defect formation is primarily induced during thermal treatment rather than during deposition. This observation supports the thermogravimetric findings later on, which demonstrate significant mass loss (~4–5%) associated with organic decomposition. The resulting volumetric shrinkage during annealing likely generates tensile stress responsible for crack formation observed in post-annealed coatings.

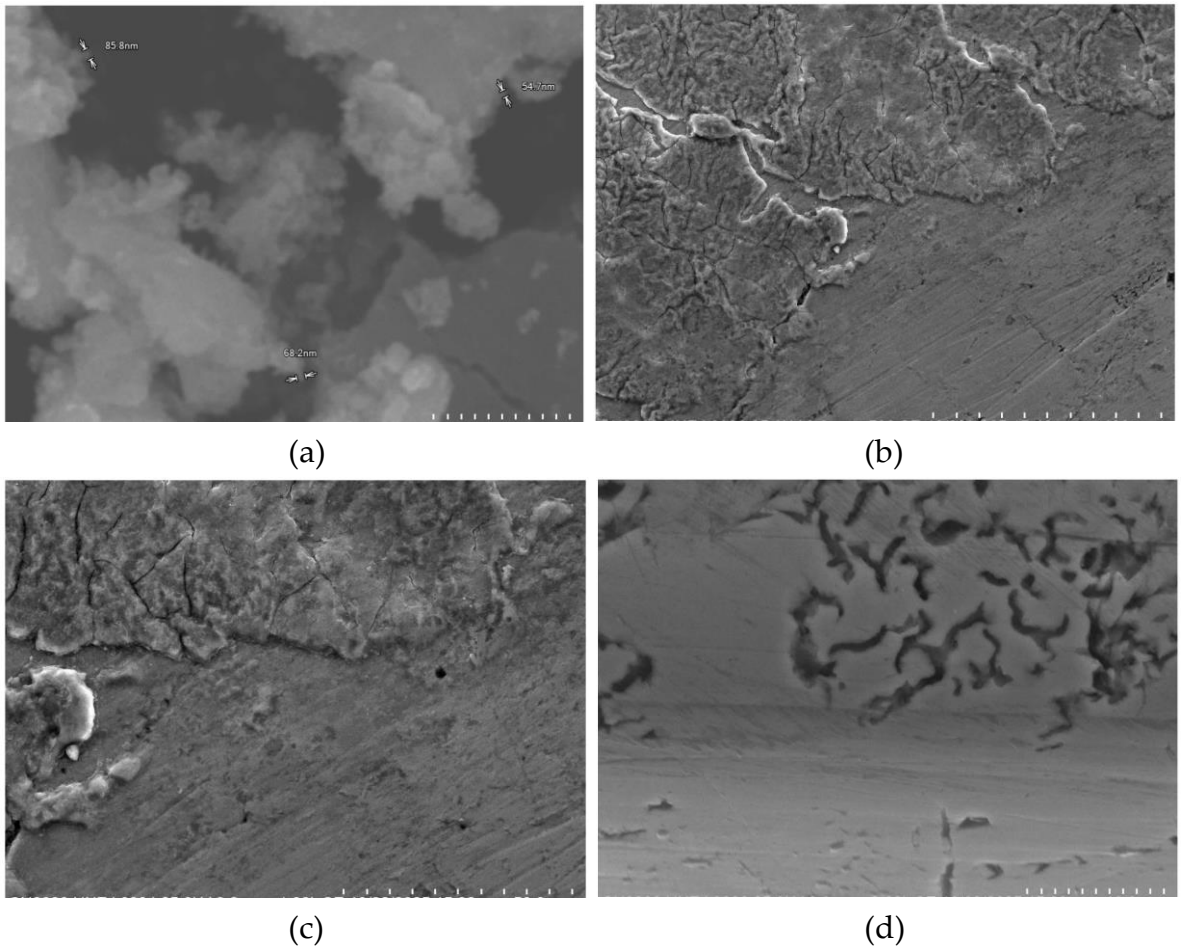

Figure 2. SEM results of ZnO Sol-Gel Coated Grey Cast Iron with (a) ×30K, (b) ×500, (c) ×1000, and (d) ×3K

The formation of cracks in sol-gel derived coatings is a well-known phenomenon and can be attributed to thermal stress, solvent evaporation, and shrinkage during the drying and calcination stages [19]. During the drying process, rapid solvent loss from the gel network produces tensile stresses on the surface, while the underlying layer remains wet, causing differential contraction. Subsequent heat treatment (calcination at 400–500 °C) further amplifies these stresses as organic residues burn out and the ZnO layer densifies. When the stress exceeds the film's cohesive strength, cracks form to relieve the stress. Additionally, the mismatch in thermal expansion coefficients between the ZnO coating and the metallic substrate (cast iron) may promote crack propagation during heating and cooling cycles.

EDS analysis, summarized in **Table 2**, confirms the presence of Zn and O as the primary elements within the coating layer, with zinc concentrations generally reaching up to ~50 wt.%, alongside ~24 wt.% oxygen and residual carbon from unreacted organic precursors. **Table 2** details the elemental composition acquired across four representative regions of the sol–gel coating, all of which confirm the formation of ZnO nanoparticles. Spectrum 1 is dominated by Zn (49.73 wt.%) and O (24.02 wt.%), with carbon residues indicating incomplete removal of organic

precursors. Spectrum 2 reveals higher Fe (8.89 wt.%), suggesting a thinner or cracked region that allowed electron beam penetration into the underlying substrate. Spectrum 3 exhibits the highest Zn content (64.38 wt.%), indicating a localized region with a thicker or more compact ZnO deposit. Spectrum 4 contains substantial Fe (20.17 wt.%) and trace Si (1.72 wt.%), further confirming non-uniform coating thickness and surface defects.

Table 2. EDS Test Results of nano-ZnO Coated Cast Iron

Spectrum	Zn (%)	O (%)	C (%)	Fe (%)	Cu (%)	Si (%)	Notes
1	49.73	24.02	24.53	1.72	–	–	ZnO detected with carbon contamination, minor Fe from substrate.
2	40.80	29.06	21.26	8.89	–	–	Higher Fe indicates thinner coating or beam penetration into metal substrate.
3	64.38	14.94	19.13	1.55	–	–	Highest Zn content—indicates thickest or densest ZnO region.
4	45.85	18.46	13.80	20.17	–	1.72	Very high Fe → coating thin or cracked; Si trace from substrate contamination.

Although cracks are present, the coating still displays good ZnO coverage and a fine-grained nanostructure, as observed at higher magnifications (10 μm scale). This indicates that the sol-gel method effectively produced a nanostructured ZnO layer, but further optimization of drying and thermal parameters is necessary to achieve a fully dense, crack-free coating suitable for tribological applications.

3.3 XRD Analysis and Structural Implications

The X-ray diffraction patterns of ZnO coatings prepared with precursor concentrations of 0.1 M, 0.2 M, and 0.4 M are presented in Figure 3. All diffraction patterns exhibit characteristic peaks corresponding to the hexagonal wurtzite ZnO structure, observed at approximately $2\theta \approx 31.7^\circ$ (100), 34.4° (002), and 36.2° (101), confirming successful crystallization of ZnO after annealing at 400 °C [20]. No additional secondary phases were detected, indicating that the sol–gel synthesis and subsequent thermal treatment effectively converted the precursor into crystalline ZnO [21].

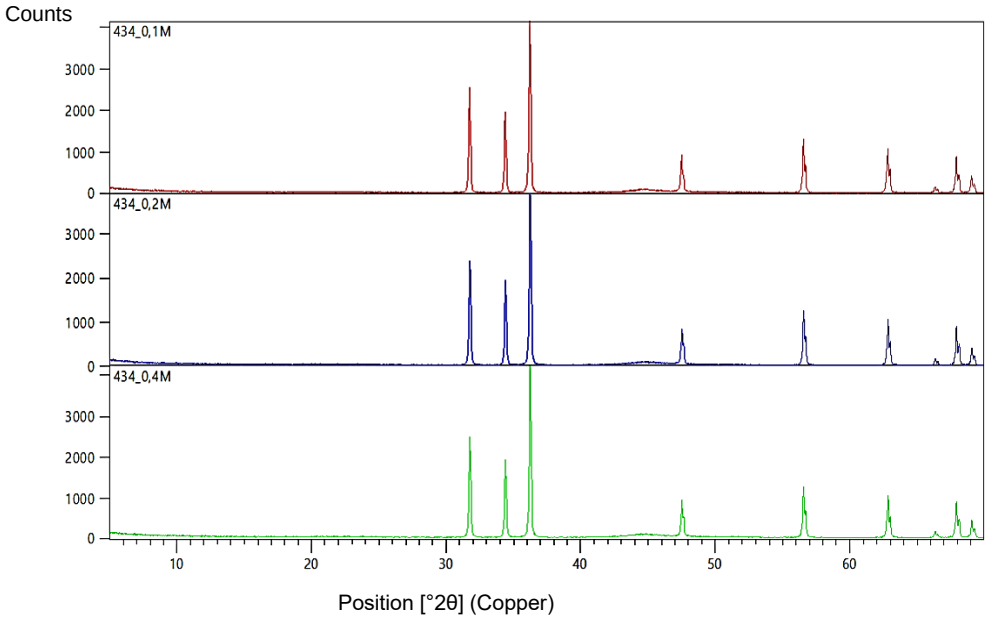

Figure 3. XRD patterns of 0.1 M, 0.2 M and 0.4 M variations of sol-gel on substrate

However, noticeable differences in peak intensity and sharpness were observed among the three molarity variations. The 0.1 M sample exhibits relatively lower peak intensity and broader diffraction peaks compared to higher molarity samples, as shown in **Figure 3**. The peak broadening observed at lower precursor concentrations suggests potential differences in crystallite size and degree of structural ordering. This behavior may be attributed to lower nucleation density and limited grain growth during annealing [22], [23].

In contrast, the 0.2 M and 0.4 M samples display sharper and more intense diffraction peaks, suggesting enhanced structural ordering and potentially larger domain sizes. The increase in precursor concentration likely enhances 〖"Zn" 〗^(2+) availability in the sol, promoting more extensive condensation reactions and denser ZnO network formation during thermal treatment. Among the three variations, the 0.4 M sample demonstrates the highest relative peak intensity.

Despite improved crystallinity at higher molarity, SEM observations revealed increased crack formation in thicker coatings. This indicates that although structural ordering improves with concentration, the accompanying increase in film thickness may lead to higher internal stresses during drying and annealing. The mismatch in thermal expansion between ZnO and the cast iron substrate, combined with volumetric shrinkage during gel-to-oxide transformation, likely contributes to crack propagation [24], [25].

The structural evolution observed from XRD correlates with the tribological findings. While higher molarity coatings exhibit better crystalline ZnO formation, their tribological performance did not consistently improve compared to the untreated control. This suggests that crystallinity alone is insufficient to guarantee

enhanced tribological behavior. Instead, coating integrity, adhesion strength, and crack density appear to play a more dominant role in determining friction and wear characteristics after annealing at 400 °C. No additional secondary phases were detected, indicating that the sol–gel synthesis and subsequent thermal treatment effectively converted the precursor into crystalline ZnO.

3.4 Thermogravimetric Analysis (TGA)

Thermogravimetric analysis was conducted to compare the thermal behavior of non-annealed (as-dried) and annealed ZnO sol–gel coatings. The non-annealed sample exhibited a total relative mass loss of approximately 4.48% upon heating, indicating the presence of residual solvents and organic precursor species that decompose during thermal exposure. This mass reduction is attributed to evaporation of physically adsorbed solvent at lower temperatures and decomposition of monoethanolamine and acetate groups at intermediate temperatures, consistent with the gel-to-oxide transformation process typical of sol–gel systems [26], [27].

In contrast, the furnaced (annealed) sample displayed a final relative mass change of approximately +4.68% over the heating range. In thermogravimetric analysis, relative mass change is defined as $\Delta m/m_0 \times 100\%$, where a positive value denotes a slight mass gain rather than a mass loss. This slight increase in mass is attributed to minor surface oxidation of the metallic FC-25 substrate under high-temperature atmosphere exposure, alongside baseline buoyancy shifts. Crucially, the absence of any continuous mass decrease (mass loss) in the thermogram verifies that residual organic solvents, monoethanolamine, and acetate precursors were completely decomposed during the preliminary 400 "°C" furnace treatment. Consequently, the coating achieves high thermal stability with no further organic degradation occurring upon subsequent reheating.

These findings validate the effectiveness of the selected annealing protocol in achieving thermally stable ZnO coatings. However, despite successful organic removal and oxide stabilization, SEM analysis revealed crack formation within the coating. This suggests that while thermal decomposition is complete, volumetric shrinkage and densification during annealing generate internal stresses that may compromise coating integrity and adversely affect tribological performance [28], [29].

3.5 Statistical Analysis

Two-way Analysis of Variance (ANOVA) was conducted to evaluate the individual and combined effects of precursor molarity (0.1 M, 0.2 M, 0.4 M) and dipping cycles (1× Dip vs. 2× Dip) on the tribological response parameters: friction force, coefficient of friction (CoF), and wear depth.

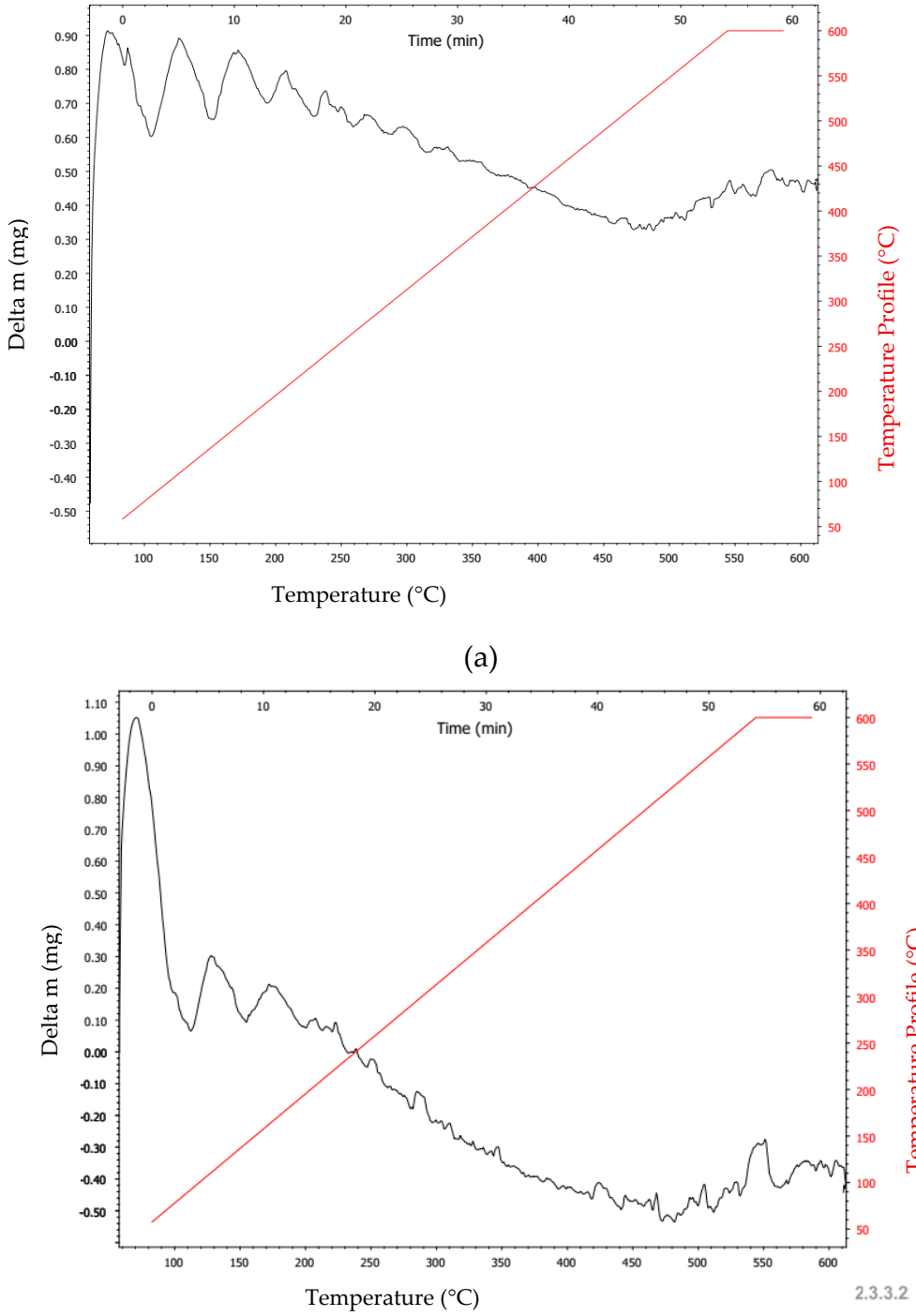

Figure 4. TGA results of sample (a) before annealing and (b) annealed

The statistical results confirm that precursor molarity exerts a statistically significant primary effect on friction and wear performance ($p < 0.05$), whereas the dipping cycle demonstrates a secondary influence. Furthermore, a statistically significant interaction between precursor molarity and dipping cycles was identified, demonstrating that precursor concentration and film thickness jointly govern coating stability and stress evolution under sliding conditions. As illustrated in the interaction plots (**Figure 5**), optimal performance among the coated specimens was obtained at intermediate-to-high molarity (0.4 M) under double dipping rather

than at extreme thickness or low molarities, confirming that managing coating integrity and defect density is critical to performance.

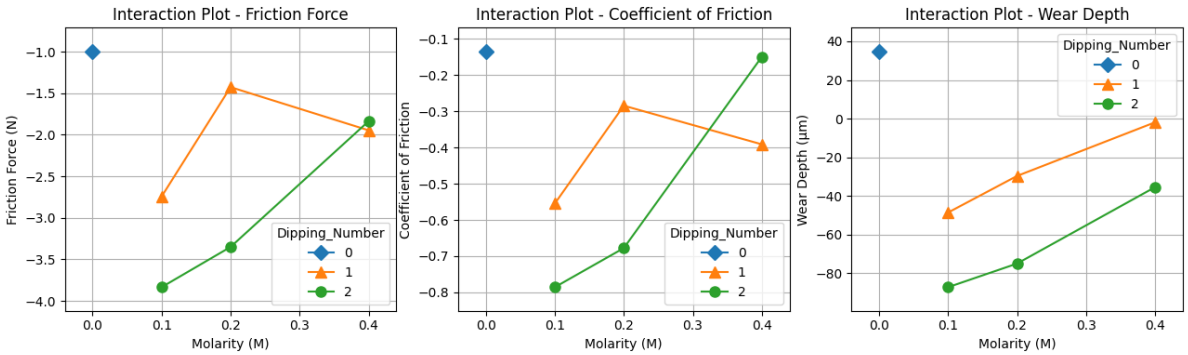

(a) (b) (c)

Figure 5. Interaction plot of (a) Friction force, (b) Coefficient of Friction and (c) Wear depth using ANOVA

The tribological results and two-way ANOVA statistically confirmed that molarity is a dominant factor influencing friction and wear, with a significant interaction between molarity and dipping number. This interaction reflects the coupled effect of precursor concentration and coating thickness on stress evolution. Optimal tribological performance was not achieved at the highest molarity, but rather under intermediate processing conditions where sufficient crystallinity was obtained without excessive crack formation. Therefore, the governing parameter for performance is not crystallinity alone, but the balance between oxide phase development and structural integrity. These findings establish that controlled precursor concentration and thickness are critical to minimizing shrinkage-induced defects and achieving mechanically stable ZnO sol–gel coatings.

3.6 Critical Considerations for Future ZnO-Based Coating Studies

The tribological and protective performance of ZnO nanoparticle coatings is governed primarily by interfacial phenomena rather than bulk crystallinity alone. Previous investigations have demonstrated that ZnO coatings can significantly reduce friction and wear when uniformly distributed and strongly adhered to the substrate surface [11], [30], [31]. However, improvements in crystallinity or phase purity, as evidenced by XRD, do not automatically translate to enhanced functional performance. Instead, coating efficiency depends critically on surface chemistry, wettability, and interfacial bonding mechanisms [32].

Surface roughness and surface energy are consistently reported as dominant parameters influencing coating adhesion. Moderate micro- or nano-scale roughness enhances mechanical interlocking and increases effective contact area, thereby improving coating stability [33]. Conversely, excessive polishing leading to near-

mirror finishes may reduce surface energy and decrease hydroxyl group density, limiting nucleation and anchoring sites for ZnO nanoparticles [34]. This phenomenon aligns with the present study, where improved surface smoothness resulted in inferior wettability prior to furnacing. Literature further indicates that controlled surface activation—through plasma treatment, chemical etching, or silane coupling—can substantially enhance adhesion by increasing surface polarity and functional group density [35], [36], [37], [38], [39], [40], [41].

Thermal treatment also plays a dual role. Furnacing improves crystallinity and removes volatile organic residues, consistent with TGA-observed mass stabilization behavior [42]. However, excessive thermal exposure may induce densification or reduce reactive surface groups necessary for chemical bonding, thereby compromising adhesion [43], [44]. Thus, thermal processing must be optimized to balance crystallinity enhancement with interfacial stability.

Collectively, both prior studies and the present findings demonstrate that ZnO coating performance is fundamentally an interfacial engineering challenge. Future researchers should prioritize: (i) controlled surface activation to increase surface energy and functional group availability; (ii) optimized roughness for mechanical interlocking; (iii) uniform nanoparticle dispersion to prevent agglomeration; and (iv) carefully optimized thermal treatment to preserve adhesion while improving structural stability. Integrating contact angle measurements, adhesion testing, and surface energy characterization alongside XRD and TGA analysis is strongly recommended for a comprehensive evaluation of coating effectiveness.

4. Conclusion

Nano-scale ZnO coatings were successfully synthesized via the sol–gel method and deposited onto FC-25 grey cast iron piston ring substrates using dip-coating followed by thermal annealing at 400 °C. Structural characterization confirmed the formation of crystalline hexagonal wurtzite ZnO, with higher precursor molarity (0.4 M) promoting enhanced crystallinity. Thermogravimetric analysis verified effective precursor decomposition, showing a 4.48% mass loss in unannealed samples and relative mass stability (+4.68%) after furnace treatment. However, SEM observations revealed microcrack formation across all annealed coatings due to volumetric shrinkage and thermal expansion mismatch.

Tribological evaluations under ASTM G99 sliding conditions demonstrated that the coated specimens did not outperform the untreated substrate control (friction force: 0.89±0.22" N" ; CoF: 0.18±0.05; wear depth: 6.6±2.1 μ"m"). Tribological performance was strongly governed by precursor molarity and dipping cycles: low-molarity double-dipped samples (2× Dip, 0.1 M) exhibited severe wear degradation (friction force: 4.91±1.55" N" ; CoF: 1.00±0.32; wear depth: 131.4±69.3 μ"m"), whereas

increasing precursor concentration (2× Dip, 0.4 M) significantly mitigated friction and wear (friction force: 1.63±0.57" N" ; CoF: 0.33±0.10; wear depth: 41.5±14.8 μ"m"). Two-way ANOVA confirmed that precursor molarity exerts a statistically significant primary effect ($p<0.05$) alongside a significant interaction with dipping cycle ($p<0.05$) on tribological parameters.

Overall, these findings demonstrate that bulk crystallinity alone is insufficient to guarantee tribological enhancement. Instead, coating structural integrity, interfacial bonding, and thermal stress management are the primary factors governing functional performance. Future work should focus on interfacial engineering, optimized heating schedules, and binder additives to eliminate defect propagation in sol–gel coatings for engine applications.

Authors' Declaration

Authors' contributions and responsibilities - The authors gratefully acknowledge the support provided by the Ministry of Higher Education, Science, and Technology (Kemendikti Saintek) of the Republic of Indonesia through the Fundamental Research - PDP (Penelitian Dosen Pemula) grant scheme. The authors also extend their appreciation to the Faculty of Engineering at Universitas Nusa Putra and Universitas Jember for providing laboratory facilities and technical assistance throughout the research. Special thanks are conveyed to the technical staff of the Materials Science Laboratory and Tribology Laboratory for their valuable contributions to sample preparation and testing procedures.

Funding - No funding information from the authors.

Availability of data and materials - All data is available from the authors.

Competing interests - The authors declare no competing interest.

Additional information - No additional information from the authors.

References

[1] K. A. H. Al Mahmud, M. A. Kalam, H. H. Masjuki, H. M. Mobarak, and N. W. M. Zulkifli, "An updated overview of diamond-like carbon coating in tribology," Crit. Rev. Solid State Mater. Sci., vol. 40, no. 2, pp. 90–118, 2015, doi: 10.1080/10408436.2014.940441.

[2] N. G. Demas, R. A. Erck, O. O. Ajayi, and G. R. Fenske, "Tribological studies of coated pistons sliding against cylinder liners under laboratory test conditions," Lubr. Sci., 2012, doi: https://doi.org/10.1002/ls.1175.

[3] S. Wang, C. Ma, and F. C. Walsh, "Alternative tribological coatings to electrodeposited hard chromium: a critical review," Trans. Inst. Met. Finish., vol. 98, no. 4, pp. 173–185, 2020, doi: 10.1080/00202967.2020.1776962.

[4] B. Ben Difallah, Y. Mebdoua, C. Serdani, M. Kharrat, and M. Dammak,

"Advanced HVOF-Sprayed Carbide Cermet Coatings as Environmentally Friendly Solutions for Tribological Applications: Research Progress and Current Limitations," Technologies, vol. 13, no. 7, 2025, doi: 10.3390/technologies13070281.

[5] D. A. Exarchos et al., "Development and characterization of environmentally friendly multifunctional protective coatings," p. 5, 2022, doi: 10.1117/12.2614989.

[6] H. Kong et al., "Multifunctional high-performance pressure/proximity/temperature sensors enabled by hybrid resistive-supercapacitive response," Nano Res., vol. 17, no. 6, pp. 5604–5613, 2024, doi: 10.1007/s12274-024-6522-8.

[7] D. M. Zhang and O. P. Kurek, "Coating Materials for Automotive Piston Rings: a Review of Tribological Performance and Engine Impact," Int. J. Res. Eng., vol. 2, no. 3, pp. 1–6, 2022, doi: 10.55640/ijre-02-03-01.

[8] M. Muruganandham et al., "Environmental applications of ZnO materials," J. Nanosci. Nanotechnol., vol. 15, no. 9, pp. 6900–6913, 2015, doi: 10.1166/jnn.2015.10725.

[9] A. H. Jayatissa, O. Ahmed, B. R. Manu, and A. M. Schroeder, "Tribological Behaviour of Sputter Coated ZnO Thin Films," Recent Prog. Mater., vol. 3, no. 1, 2021, doi: 10.21926/rpm.2101003.

[10] B. Ren et al., "Tribological properties and anti-wear mechanism of ZnO@graphene core-shell nanoparticles as lubricant additives," Tribol. Int., vol. 144, no. November 2019, 2020, doi: 10.1016/j.triboint.2019.106114.

[11] S. V. Katoch, T. Kapil, D. Maheshwari, and G. Jindal, "Investigating the effect of zinc oxide nanoparticle coverings in reducing frictional wear and tear in tribological systems," vol. 22, no. 2, pp. 277–290, 2025.

[12] P. Shafiee, M. Reisi Nafchi, S. Eskandarinezhad, S. Mahmoudi, and E. Ahmadi, "Sol-gel zinc oxide nanoparticles: advances in synthesis and applications," Synth. Sinter., vol. 1, no. 4, 2021, doi: 10.53063/synsint.2021.1477.

[13] U. Chibuzoh and N. Skat, "New Sol-Gel Coatings to Improve Casting Quality A PhD Thesis By Ugochukwu Chibuzoh Nwaogu Supervisor : Niels Skat Tiedje , PhD .," 2011.

[14] P. Puspitasari, A. A. Permanasari, A. Warestu, G. P. P. Arifiansyah, D. D. Pramono, and T. Pasang, "Tribology Properties on 5W-30 Synthetic Oil with Surfactant and Nanomaterial Oxide Addition," Automot. Exp., vol. 6, no. 3, pp. 669–686, 2023, doi: 10.31603/ae.10115.

[15] AMERICAN SOCIETY FOR TESTING AND MATERIALS, "Astm G99-17," Stand. Test Method Wear Test. with a Pin-on- Disk Appar., vol. 05, no. 2016, pp. 1–6, 2017, doi: 10.1520/G0099-17.Copyright.

[16] K. Wojtasik et al., "Zinc Oxide Films Fabricated via Sol-Gel Method and Dip-Coating Technique-Effect of Sol Aging on Optical Properties, Morphology and Photocatalytic Activity.," Mater. (Basel, Switzerland),

vol. 16, no. 5, Feb. 2023, doi: 10.3390/ma16051898.

[17] A. Ramdas Bari, P. Anil Bari, and R. H. Bari, "Studies on sol-gel dip-coated nanostructured ZnO thin films," J. Nanostructures, vol. 9, no. 2, pp. 326–330, 2019, doi: 10.22052/JNS.2019.02.014.

[18] A. Elagouz, M. K. A. Ali, H. Xianjun, M. A. A. Abdelkareem, and M. A. Hassan, "Frictional performance evaluation of sliding surfaces lubricated by zinc-oxide nano-additives," Surf. Eng., vol. 36, no. 2, pp. 144–157, 2020, doi: 10.1080/02670844.2019.1620442.

[19] E. J. Kappert, D. Pavlenko, J. Malzbender, A. Nijmeijer, N. E. Benes, and P. A. Tsai, "Formation and prevention of fractures in sol-gel-derived thin films," Soft Matter, vol. 11, no. 5, pp. 882–888, 2015, doi: 10.1039/c4sm02085e.

[20] R. C and A. Arulraj, "Enhanced photoconductive response of ZnO thin films with the impact of annealing temperatures on structural and optical properties," Sci. Rep., vol. 15, no. 1, 2025, doi: 10.1038/s41598-025-02177-7.

[21] T. D. Malevu and R. O. Ocaya, "Effect of annealing temperature on structural, morphology and optical properties of ZnO nano-needles prepared by zinc-air cell system method," Int. J. Electrochem. Sci., vol. 10, no. 2, pp. 1752–1761, 2015, doi: 10.1016/s1452-3981(23)05109-x.

[22] D. Aryanto et al., "Preparation and structural characterization of ZnO thin films by sol-gel method," J. Phys. Conf. Ser., vol. 817, no. 1, 2017, doi: 10.1088/1742-6596/817/1/012025.

[23] Y. Rama Denny Muchtar, T. Firmansyah, A. Trenggono, D. Wijaya, G. Antarnusa, and A. Suherman, "Effect of Precursor Concentration and Annealed Substrate Temperature on the Crystal Structure, Electronic and Optical Properties of ZnO thin film," J. Pure Appl. Chem. Res., vol. 9, no. 1, pp. 57–65, 2020, doi: 10.21776/ub.jpacr.2020.009.01.514.

[24] A. Arslanov, S. Yuldashev, N. Botirova, R. Nusretov, J. Murodov, and J. Xudoyqulov, "Impact of Precursor Molar Concentration on the Structural and Optical Properties of ZnO Thin Films Synthesized by Ultrasonic Spray Pyrolysis," Phys. Sci. Int. J., vol. 29, no. 1, pp. 29–35, 2025, doi: 10.9734/psij/2025/v29i1871.

[25] Y. Kim and J. Y. Leem, "Effects of precursor concentration on structural and optical properties of ZnO thin films grown on muscovite mica substrates by sol-gel spin-coating," J. Nanosci. Nanotechnol., vol. 16, no. 5, pp. 5186–5189, 2016, doi: 10.1166/jnn.2016.12267.

[26] A. Gómez-Núñez, S. Alonso-Gil, C. López, P. Roura-Grabulosa, and A. Vilà, "From ethanolamine precursor towards ZnO—How N is released from the experimental and theoretical points of view," Nanomaterials, vol. 9, no. 10, 2019, doi: 10.3390/nano9101415.

[27] A. Rahman et al., "Bioremediation of hexavalent chromium (VI) by a soil-borne bacterium, Enterobacter cloacae B2-DHA," J. Environ. Sci. Heal. - Part A Toxic/Hazardous Subst. Environ. Eng., vol. 50, no. 11, pp. 1136 – 1147, 2015, doi: 10.1080/10934529.2015.1047670.

[28] A. Fabrizi et al., "Thermal stability of nanostructured coatings," Mater. Sci. Forum, vol. 653, pp. 1–22, 2010, doi: 10.4028/www.scientific.net/MSF.653.1.

[29] D. Kamaruzaman et al., "Effects of Thermal Annealing on The Morphology and Structural Characteristics of Zinc Oxide Nanopowders for Triboelectric Nanogenerator Applications," J. Adv. Res. Fluid Mech. Therm. Sci., vol. 99, no. 1, pp. 17–27, 2022, doi: 10.37934/arfmts.99.1.1727.

[30] S. A. Farooq, A. Raina, S. Mohan, R. A. Singh, S. Jayalakshmi, and M. I. U. Haq, "Nanostructured Coatings: Review on Processing Techniques, Corrosion Behaviour and Tribological Performance," Nanomaterials, vol. 12, no. 8, 2022, doi: 10.3390/nano12081323.

[31] R. Gholami, H. G. Kashani, M. Silani, and S. Akbarzadeh, "Experimental and numerical investigation of friction coefficient and wear volume in the mixed-film lubrication regime with ZnO nano-particle," J. Appl. Fluid Mech., vol. 13, no. 3, pp. 993–1001, 2020, doi: 10.29252/JAFM.13.03.30645.

[32] C. Wang, G. O. Brown, D. L. Burris, L. S. T. J. Korley, and T. H. Epps, "Coating Architects: Manipulating Multiscale Structures to Optimize Interfacial Properties for Coating Applications," ACS Appl. Polym. Mater., vol. 1, no. 9, pp. 2249–2266, 2019, doi: 10.1021/acsapm.9b00302.

[33] S. G. Croll, "Surface roughness profile and its effect on coating adhesion and corrosion protection: A review," Prog. Org. Coatings, vol. 148, 2020, doi: 10.1016/j.porgcoat.2020.105847.

[34] D. E. Packham, "Handbook of Adhesion: Second Edition," Handb. Adhes. Second Ed., pp. 1–638, 2005, doi: 10.1002/0470014229.

[35] V. Purcar et al., "The effect of different coupling agents on nano-ZnO materials obtained via the sol-gel process," Nanomaterials, vol. 7, no. 12, 2017, doi: 10.3390/nano7120439.

[36] R. Wolf and A. C. Sparavigna, "Role of Plasma Surface Treatments on Wetting and Adhesion," Engineering, vol. 02, no. 06, pp. 397–402, 2010, doi: 10.4236/eng.2010.26052.

[37] M. Kumar and C. Sasikumar, "Electrodeposition of Nanostructured ZnO Thin Film: A Review," Am. J. Mater. Sci. Eng., vol. 2, no. 2, pp. 18–23, 2014, doi: 10.12691/ajmse-2-2-2.

[38] B. Xie, Y. Ma, J. Wang, Y. Liu, and R. Yin, "Chemical Cross-Linking Cellulose Aerogel-Based Triboelectric Nanogenerators for Energy Harvesting and Sensing Human Activities," ACS Appl. Mater. Interfaces, vol. 16, no. 15, pp. 19411–19420, 2024, doi: 10.1021/acsami.4c02671.

[39] K. Vyavhare, R. B. Timmons, A. Erdemir, B. L. Edwards, and P. B. Aswath, "Robust Interfacial Tribofilms by Borate- A nd Polymer-Coated ZnO Nanoparticles Leading to Improved Wear Protection under a Boundary Lubrication Regime," Langmuir, vol. 37, no. 5, pp. 1743–1759, 2021, doi: 10.1021/acs.langmuir.0c02985.

[40] R. Amari, A. Mahroug, A. Boukhari, B. Deghfel, and N. Selmi, "Structural, Optical and Luminescence Properties of ZnO Thin Films Prepared by Sol-Gel Spin-Coating Method: Effect of Precursor Concentration," Chinese Phys. Lett., vol. 35, no. 1, 2017, doi: 10.1088/0256-307X/35/1/016801.

[41] A. K. Guin, M. Bhadu, M. Sinhababu, T. K. Rout, and G. Udayabhanu, "Effect of nano-ZnO containing sol-gel coating on galvanised iron sheet," Pigment Resin Technol., vol. 44, no. 4, pp. 239–249, 2015, doi: 10.1108/PRT-01-2014-0007.

[42] D. Weber, S. Botnaraş, D. V. Pham, J. Steiger, and L. De Cola, "Functionalized ZnO nanoparticles for thin-film transistors: Support of ligand removal by non-thermal methods," J. Mater. Chem. C, vol. 1, no. 18, pp. 3098–3101, 2013, doi: 10.1039/c3tc00576c.

[43] H. T. Dao and H. Makino, "Effects of substrate temperature on thermal stability of Al-doped ZnO thin films capped by AlOx," Ceram. Int., vol. 47, no. 6, pp. 8060–8066, 2021, doi: 10.1016/j.ceramint.2020.11.160.

[44] R. Khanna, K. Ip, Y. W. Heo, D. P. Norton, S. J. Pearton, and F. Ren, "Thermal degradation of electrical properties and morphology of bulk single-crystal ZnO surfaces," Appl. Phys. Lett., vol. 85, no. 16, pp. 3468–3470, 2004, doi: 10.1063/1.1801674.